

Experimental realization of universal high-dimensional quantum gates with ultra-high fidelity and efficiency

Zhe Meng,^{*} Wen-Qiang Liu,^{*} Bo-Wen Song, Xiao-Yun Wang, An-Ning Zhang,[†] and Zhang-Qi Yin[‡]

Center for Quantum Technology Research and Key Laboratory of
Advanced Optoelectronic Quantum Architecture and Measurements (MOE),
School of Physics, Beijing Institute of Technology, Beijing 100081, China

(Dated: December 1, 2023)

Qudit, a high-dimensional quantum system, provides a larger Hilbert space to process the quantum information and has shown remarkable advantages over the qubit counterparts. It is a great challenge to realize the high fidelity universal quantum gates with qudits. Here we theoretically propose and experimentally demonstrate a set of universal quantum gates for a single optical qudit with four dimensions (including the generalized Pauli X_4 gate, Pauli Z_4 gate, and all of their integer powers), which are encoded in the polarization-spatial degree of freedom without multiple unstable cascaded interferometers. Furthermore, we also realize the controlled- X_4 gate and all of its integer powers. We have achieved both the ultra-high average gate fidelity 99.73% and efficiency 99.47%, which are above the error threshold for fault-tolerant quantum computation. Our work paves a way for the large-scale high-dimensional fault-tolerant quantum computation with a polynomial resource cost.

Introduction.—Universal quantum logic gates are essential building blocks in many quantum information processing tasks [1]. Recently, the realization of qubit-based quantum gates in many physical platforms has been theoretically developed and experimentally demonstrated well [2–8]. In addition to qubit, qudit with d -ary ($d > 2$) digits has emerged as a richer resource in high-dimensional quantum systems and it has been extended to high-dimensional logic to encode and process quantum information [9, 10]. Due to the larger operation space, qudit quantum systems have shown their remarkable advantages. For example, simplifying quantum gates [11–14], improving the efficiency of fault-tolerant quantum computation [15, 16], increasing channel capacity [17–20], improving communication security [21–23], etc. Besides, the qudits can exceed the limitations imposed by the qubits in larger violation of Bell-type inequality [24–26] and higher noise resilience [27–29]. Up to now, qudit-based quantum information processing has been reported and experimentally implemented in various physical systems [30–38]. Though high-dimensional quantum information processing has made significant progress, a lot of efforts still are required for improving the quantum gates fidelity [30, 31].

Photon is a natural candidate for encoding the qudit due to its various degrees of freedom (DOFs). There are many experiments that have been demonstrated universal quantum gates for the qudits, which are formed by the orbital angular momentum (OAM) [39–42], the time-frequency DOF [43], or the spatial modes of photons [44, 45]. In 2017, Babazadeh *et al.* experimentally demonstrated a four-dimensional generalized Pauli X_4 gate and all of its integer powers with a conversion efficiency of 87.3% and a fidelity of 93.4% using the OAM mode of a single photon [39]. Later, Wang *et al.* improved the conversion efficiency to 93% [42]. In 2022, Chi *et al.* experimentally realized the Pauli X_4 gate with

the fidelity of 98.8% and a four-dimensional controlled- X_4 gate with the fidelity of 95.2% on a programmable silicon-photon quantum processor [45]. In all above works [39–42, 45], the experimental realization of the high-dimensional quantum gates depends on either the multiple Sagnac-type interferometers or multiple Mach-Zehnder-type interferometers, which are both faced with the great challenges of phase instability. Therefore, the fidelity and efficiency of the universal quantum gates for the optical qudits are significantly degraded, compared to their qubit counterparts [46–48].

In this Letter, we experimentally demonstrate a universal four-dimensional quantum gate set on the single photons carrying both the polarization and the spatial mode DOFs. The gate set includes the four-dimensional Pauli X_4 gate, Pauli Z_4 gate, and all of their integer powers, which can efficiently construct any four-dimensional quantum operations. The Pauli X_4 gate, Pauli Z_4 gate, and all of their integer powers are realized with the polarization-spatial DOF of the single photons. We also realize the controlled- X_4 gate and all of its integer powers. Our experiments overcome the obstacles of phase instability and greatly simplify the previous works based on many cascaded interferometers [39–42, 45]. The experimental results show both ultra-high ($\sim 99.5\%$) gate efficiency and fidelity, which are above error threshold for fault-tolerant quantum computation [49, 50].

High-dimensional quantum gates.—A qudit quantum gate is described in a d -dimensional Hilbert space \mathcal{H}_d that is spanned by a set of orthogonal bases $\{|0\rangle, |1\rangle, \dots, |d-1\rangle\}$. The most important d -dimensional quantum gates are the generalized single-qudit Pauli X_d gate, Pauli Z_d gate, two-qudit controlled- X_d gate, and all their integer powers. These gates are universal and they can construct arbitrary high-dimensional unitary transformations [10, 39]. The transformations of the d -dimensional single-qudit n (an integer number) powers

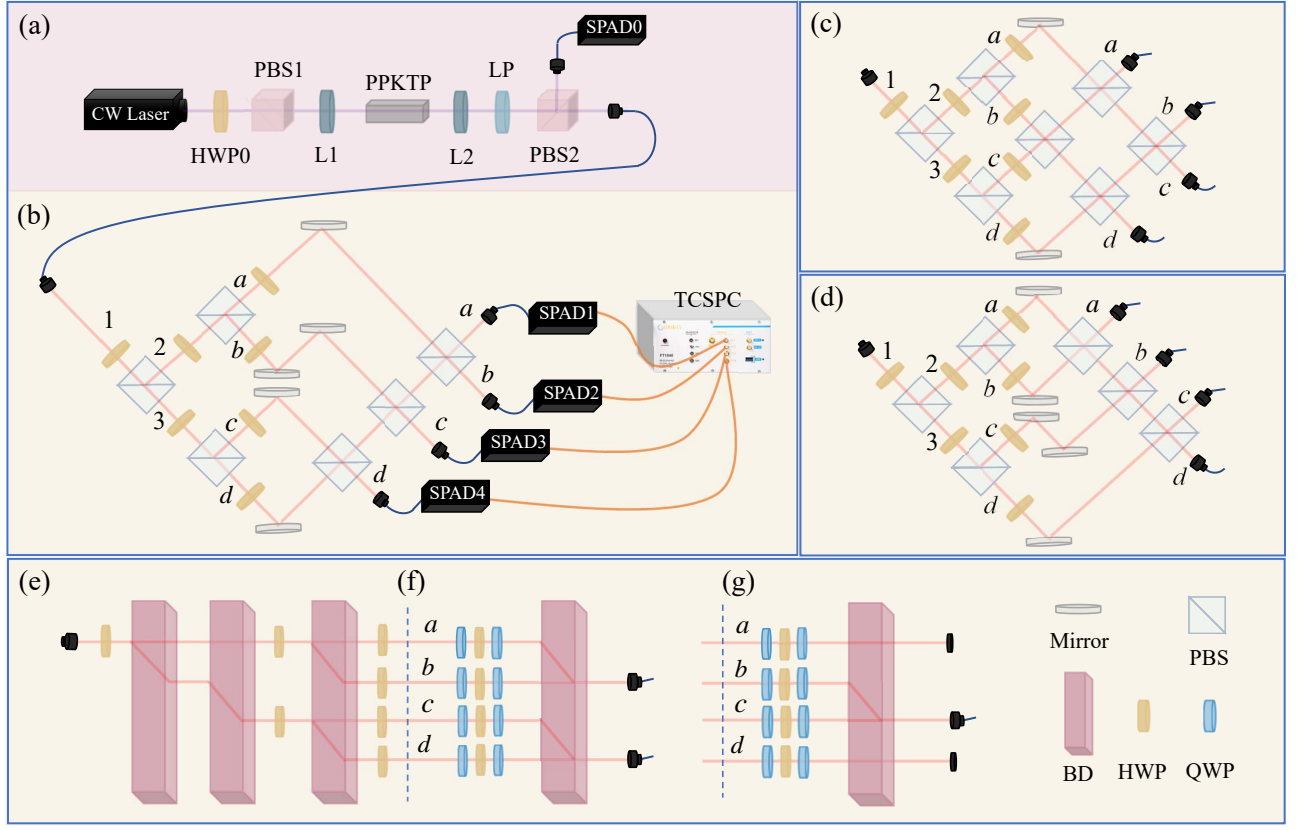


FIG. 1. Schematic of the experimental setup for realization of the generalized four-dimensional Pauli X_4 gate, Pauli Z_4 gate and all of their integer powers. (a) The preparation of a heralded single-photon source. The experimental setups for the realization of (b) X_4 gate, (c) X_4^2 gate, and (d) X_4^3 gate, where the optical elements before the mirrors present the initial state preparation and the optical elements after the mirrors describe the gate operations. (e)-(g) The experimental setups for the realization of Pauli Z_4 , Z_4^2 , Z_4^3 gates. (e) The initial state preparation of the Z_4 , Z_4^2 , Z_4^3 gates. (f)-(g) The implementation of the Pauli Z_4 , Z_4^2 , Z_4^3 gates and the measurement of the phase differences in spatial modes a and b , c and d , b and c . The effective coincidence window (including the jitter of the detector) is about 2 ns.

of Pauli X_d (X_d^n) gate and n powers of Z_d (Z_d^n) gate on the d -dimensional quantum state are expressed by [51]

$$X_d^n |l\rangle = |l \oplus n\rangle_{\text{mod } d}, \quad Z_d^n |l\rangle = \omega^{n \cdot l} |l\rangle. \quad (1)$$

Here $l \in \{0, 1, \dots, d-1\}$, $|l \oplus n\rangle_{\text{mod } d} = (l+n) \text{ modulo } d$, and $\omega = \exp(2\pi i/d)$. The X_d^n gate is a cyclic operation in which each quantum state is transformed to its n -th nearest state in a clockwise direction. The Z_d^n gate is a phase operation in which each quantum state is introduced a state-dependent phase. The generalized n powers of Pauli Y_d (Y_d^n) gate can be given by $Y_d^n = X_d^n Z_d^n$. When $n=1$ and $d=2$, they would simplify to qubit Pauli X gate, Pauli Y gate, and Pauli Z gate. Besides, the important two-qudit gate is the controlled- X_d^n (CX_d^n) gate, which is formulated as [10]

$$CX_d^n (|k\rangle|l\rangle) = |k\rangle|k \oplus l \oplus (n-1)\rangle_{\text{mod } d}. \quad (2)$$

The CX_d^n gate realizes a cyclic operation on the target qudit $|l\rangle$ by manipulating the value of the controlled qudit $|k\rangle$ and leaves it unchanged on the controlled qudit.

In qubit version, the CX_d^n gate becomes the well-known controlled-NOT (CNOT) gate.

Experimental setup.—Quantum gates X_4 , X_4^2 , X_4^3 ($X_4^\dagger = X_4^3$) and Z_4 , Z_4^2 , Z_4^3 ($Z_4^\dagger = Z_4^3$) are sufficient to construct arbitrary quantum operations in the four-dimensional space. The experimental setup for the realization of these elementary gates is shown in Fig. 1, where the gate qudit is encoded on the polarization-spatial DOF of the single photons, i.e., $|0\rangle \leftrightarrow |Ha\rangle$, $|1\rangle \leftrightarrow |Hb\rangle$, $|2\rangle \leftrightarrow |Hc\rangle$, and $|3\rangle \leftrightarrow |Hd\rangle$. The horizontally H -polarized DOF of photons controls the spatial mode DOF (a, b, c, d) of photons to route the photons into the corresponding logic gates by using some linear optical elements.

Figure 1(a) illustrates a heralded single-photon source, in which a continuous-wave diode laser (CW Laser) is employed to generate a pump laser beam with a central wavelength of 405 nm and an output power of 20 mW. This pump laser is utilized for the production of photon

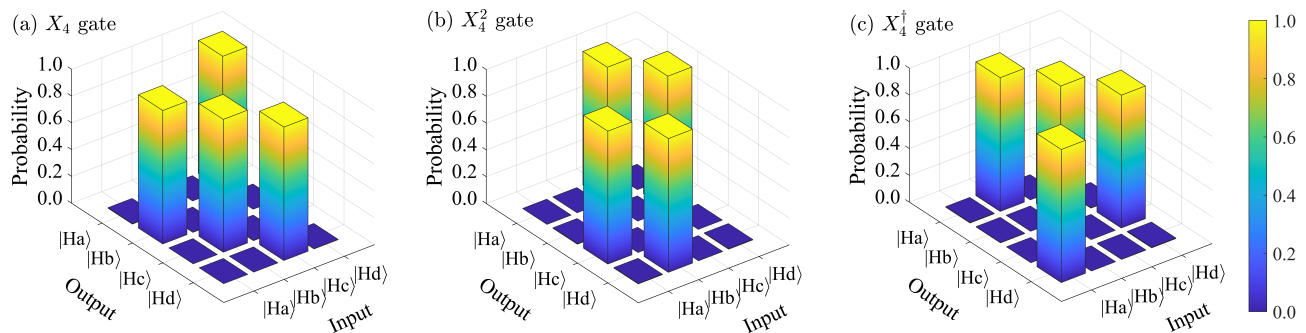


FIG. 2. Truth tables for (a) X_4 gate, (b) X_4^2 gate, and (c) X_4^\dagger gate. After preparing a qudit in one of the four input computational basis from $|Ha\rangle$ to $|Hd\rangle$, the probabilities of all output basis states are measured in 10s. The average conversion efficiencies of truth tables for X_4 gate, X_4^2 gate and X_4^\dagger gate are 0.9941, 0.9961, and 0.9950, respectively.

pairs at a wavelength of 810 nm through type-II spontaneous parametric down-conversion in a periodically poled potassium titanyl phosphate (PPKTP) crystal. A half-wave plate (HWP0) and a polarization beam splitter (PBS1) are used to regulate optical power, and two lenses (L1 and L2) placed before and after the PPKTP crystal are used to focus and collimate beams. Then, the photon pairs are filtered at a long pass filter (LP) to eliminate any residual pumped laser light and they finally are split at PBS2. During this process, one photon from each pairs is detected at single-photon avalanche photodiode (SPAD0) to serve as a herald idler photon, and the other photon from pairs as signal photon H is injected into a four-dimensional Pauli X_4 gate in Fig. 1(b).

As shown in Fig. 1(b), the $|H\rangle$ photon firstly goes through a HWP in spatial mode 1 to evolve the H -polarized photon into the superposition of the horizontally H -polarized photon and vertically V -polarized photon. Then a PBS reflects the V -polarized photon into the spatial mode 2 and transmits the H -polarized photon into the spatial mode 3. Subsequently, the photons in spatial modes 2 and 3 go through HWPs, PBSs, and HWPs respectively, in which the PBSs divide the photons into the spatial modes a , b , c , d . Because the parameters of the HWPs can be adjusted arbitrarily, the four-dimensional Hilbert space is spanned by the trajectories of photons in a , b , c , and d , which generates a general superposition of polarization-spatial states (see Supplementary Materials)

$$\alpha|Ha\rangle + \beta|Hb\rangle + \gamma|Hc\rangle + \delta|Hd\rangle. \quad (3)$$

Here the complex coefficients α , β , γ , and δ satisfy the normalization condition $|\alpha|^2 + |\beta|^2 + |\gamma|^2 + |\delta|^2 = 1$. After the initial state is prepared, the photon is routed to a X_4 gate that is composed of three PBSs, which evolves the initial state in Eq. (3) as

$$\alpha|Hb\rangle + \beta|Hc\rangle + \gamma|Hd\rangle + \delta|Ha\rangle. \quad (4)$$

From Eq. (3) to Eq. (5), one can see that the X_4 gate is accomplished. In this way, the X_4^2 gate and X_4^\dagger gate also can be realized by routing the photon to different spatial modes using the PBSs, and the corresponding experimental setups are presented in Fig. 1(c) and Fig. 1(d), respectively.

Our four-dimensional universal quantum gates exhibit advantages over quantum walk. In our experiment, X gate can transit from the spatial mode d to the spatial mode a using merely three PBSs. The quantum walk scheme requires three steps to complete, which is an operation that requires fifteen PBSs and thirty HWPs. This is primarily due to the fact that the number of optical elements required for quantum walk increases polynomially with the number of steps. In the quantum walk scheme, a d -dimensional Pauli X_d gate and CX_d gate can be realized by using $(1.5d^2 - 2.5d + 1)$ PBSs and $(3d^2 - 5d + 2)$ HWPs [52–54].

We also experimentally realize the Pauli Z_4 , Z_4^2 , and Z_4^\dagger gates shown in Figs. 1(e)-(g). Specifically, Fig. 1(e) presents the initial state preparation using the beam displacers (BDs) and HWPs, which can be modeled as a general state in Eq. (3). In this case, it is equivalent to the method of using PBSs and HWPs for the initial state preparation of the X_4 gate. Figs. 1(f)-(g) show the gate operations and the relative phase measurements, where a combination of two quarter-wave plates (QWPs) and one HWP is used to introduce the state-dependent phase operations in corresponding spatial modes, and finally measuring the relative phase between two pairwise locations by the interference of the photons from the spatial modes a and b , c and d , b and c , respectively.

In experiments, the output signal photons after the gate operations are detected by a measurement device consisting of four SPADs (SPAD1, SPAD2, SPAD3, SPAD4) and a time-correlated single photon counting (TCSPC). This allows the photon number statistics in each output spatial modes to count the probabilities of all four elementary output bases for the Pauli X_4 , X_4^2 ,

TABLE I. The in-out efficiency $\mathcal{P}(i, j)$ for the X_4 , X_4^2 , and X_4^\dagger gates in our experimental setups.

Input mode	$ Ha\rangle$	$ Hb\rangle$	$ Hc\rangle$	$ Hd\rangle$
X_4 gate	99.58%	99.13%	99.60%	99.31%
X_4^2 gate	99.19%	99.84%	99.96%	99.46%
X_4^\dagger gate	99.33%	99.81%	99.77%	99.11%

X_4^\dagger gates, and it also ascertains the relative phases between pairwise output spatial modes for the Pauli Z_4 , Z_4^2 , Z_4^\dagger gates. This measurement process is sustained over a duration of 10 seconds by registering the coincidence between the SPAD1, SPAD2, SPAD3, SPAD4 and triggering SPAD0, respectively. For each measurement, we record the detection of approximately 9000 heralded single photons by registering the clicks over a duration of 1 second.

Experimental results.—The conversion efficiency and gates fidelity can be used to evaluate the performance of the quantum gates. The conversion efficiency of the gate is defined as $\mathcal{P}(i, j) = n_{ij} / \sum_k n_{ik}$. Here n_{ij} denotes the output photon number in the j -th spatial mode when the input photon is in the i -th spatial mode, and $\sum_k n_{ik}$ denotes the summation over the photon number in all possible output spatial modes when the input photon is in the i -th spatial mode. We reconstruct the truth tables for the X_4 , X_4^2 , and X_4^\dagger gates plotted in Fig. 2, which describe the population of all computational basis output states to each of the computational basis input states. We calculate the efficiencies of the X_4 , X_4^2 , and X_4^\dagger gates and list them in Tab. I. The average efficiencies of the X_4 , X_4^2 , and X_4^\dagger gates are 99.41%, 99.61%, 99.50%, respectively. The experimental errors stem mainly from the imperfections of the single photon source and the single photon detectors.

In order to check the transformations are quantum gates instead of classical gates, we need to input the four-dimensional state in a quantum superposition way. In experiments, we send the photons prepared in an equal superposition state into the gate operations and then measure the output state. We calculate the gate fidelity $\mathcal{F}(\rho_e, \rho_t) = \text{Tr}(\sqrt{\sqrt{\rho_e}\rho_t\sqrt{\rho_e}})$ between the experimental output state ρ_e and the theoretical output state $\rho_t = U\rho_i U^\dagger$ (ρ_i is input state and U is the transformation of the gates) [1]. We find that the fidelities for X_4 , X_4^2 , and X_4^\dagger gates are $\mathcal{F}_{X_4} = 99.70\%$, $\mathcal{F}_{X_4^2} = 99.80\%$, and $\mathcal{F}_{X_4^\dagger} = 99.75\%$, which go beyond significantly the maximum fidelity for these classical gates bounded by $\mathcal{F}_{cl} = 49.82\%$ in our experiments [39]. These results suggest the gates run with ultra-high quality in a coherent way and it can also obtain the similar outcome for the other possible coherent superpositions.

Figure 3 shows the experimental density matrix for the Z_4 gate in an input equal superposition state, where the

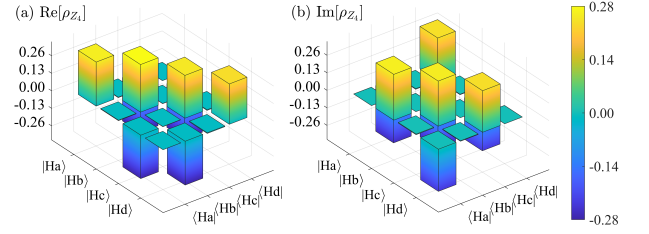


FIG. 3. The reconstructed density matrix ρ_{Z_4} for the Z_4 gate. (a) and (b) are the real part and the imaginary part of the density matrix for the Z_4 gate, respectively. The fidelity of the Z_4 gate is 99.81%.

real and imaginary parts are reconstructed in Fig. 3(a) and Fig. 3(b), respectively. The density matrices for Z_4^2 gate and Z_4^\dagger gate can be found in Supplementary Materials. We obtain the fidelity of the Z_4 , Z_4^2 and Z_4^\dagger gates $\mathcal{F}_{Z_4} = 99.81\%$, $\mathcal{F}_{Z_4^2} = 99.55\%$, and $\mathcal{F}_{Z_4^\dagger} = 99.83\%$. Besides, by adjusting the angles of the HWPs for the initial state preparation in Figs. 1(b)-(d), we also experimentally realize the high-dimensional controlled-cyclic gates where the controlled qubits are encoded on the polarization states and the target qudits are encoded on the spatial mode states. The controlled-cyclic (CX_4^n) gate in an eight-dimensional hybrid Hilbert space is expressed by

$$CX_4^n = |V\rangle\langle V| \otimes I_4 + |H\rangle\langle H| \otimes X_4^n. \quad (5)$$

Here I_4 is a four-dimensional identical operation. When the control qubit is V -polarized photon, the CX_4^n gate preforms an I_4 operation and when the control qubit is H -polarized photon, the CX_4^n gate preforms a X_4^n operation. We initiate the preparation of a qudit in one of the eight elementary basis input states from $|Va\rangle, \dots, |Vd\rangle, |Ha\rangle, \dots, |Hd\rangle$, and execute a measurement procedure to count the probabilities of all eight elementary output states. The experimental truth table of the CX_4 gate is presented in Fig. 4 with an average conversion efficiency of 99.25%. The average efficiencies of the CX_4^2 and CX_4^\dagger gates are 99.56%, and 99.47%, and their truth tables can be found in Supplementary Materials. We also obtain the fidelities for all these gates in an equal superposition input state, which are given by $\mathcal{F}_{CX_4} = 99.62\%$, $\mathcal{F}_{CX_4^2} = 99.78\%$, and $\mathcal{F}_{CX_4^\dagger} = 99.73\%$.

Conclusion.—We have investigated the implementations of four-dimensional generalized Pauli X_4 gate, Z_4 gate, and all of their integer powers based on the polarization-spatial DOF of the single photon. These quantum gates form a completed basis in the four-dimensional Hilbert space, which can construct arbitrary four-dimensional quantum operations. Besides, we also realized the controlled- X_4 gate and its all integer powers. Our experimental setups greatly simplify the implementations of these gates and the experimental results show

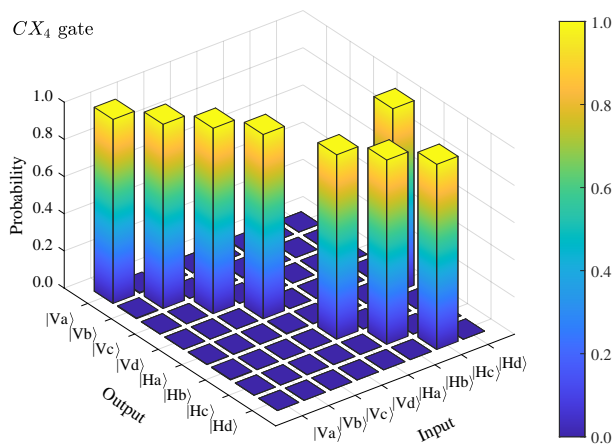


FIG. 4. Truth tables for the CX_4 gate. The average efficiency of the CX_4 gate is 99.25%.

both the ultra-high fidelity and efficiency, which improves significantly the previous works based on OAM [39–42].

These elementary high-dimensional quantum gates have important applications in many high-dimensional quantum information processing tasks, such as the preparation of high-dimensional entangled states [55], high-dimensional quantum key distribution [56], high-dimensional quantum teleportation [57], and quantum information transfer [58]. Our experiments can easily scale up more spatial modes to realize any higher-dimensional quantum operations. In this way, a d -dimensional Pauli X_d gate and CX_d gate can be realized by using $d - 1$ PBSs, and a d -dimensional Pauli Z_d gate can be realized by using d HWPs and $2d$ QWPs. The work opens up a new way to construct a large-scale qudit-based photonic chip quantum processor with a polynomial resource cost [45].

This work is supported by National Natural Science Foundation of China (Grant No.92365115), Beijing Institute of Technology Research Fund Program for Young Scholars.

* These two authors contributed equally to this work.

† Corresponding author. Anningzhang@bit.edu.cn

‡ Corresponding author. zqyin@bit.edu.cn

- [1] M. A. Nielsen and I. L. Chuang, *Quantum computation and quantum information* (Cambridge university press, Cambridge, England, 2010).
- [2] E. Knill, R. Laflamme, and G. J. Milburn, A scheme for efficient quantum computation with linear optics, *Nature* **409**, 46 (2001).
- [3] J. L. O’Brien, G. J. Pryde, A. G. White, T. C. Ralph, and D. Branning, Demonstration of an all-optical quantum controlled-NOT gate, *Nature* **426**, 264 (2003).
- [4] Z. Zhao, A. N. Zhang, Y. A. Chen, H. Zhang, J. F. Du, T. Yang, and J. W. Pan, Experimental demonstration of

a nondestructive controlled-NOT quantum gate for two independent photon qubits, *Phys. Rev. Lett.* **94**, 030501 (2005).

- [5] J. Zeuner, A. N. Sharma, M. Tillmann, R. Heilmann, M. Gräfe, A. Moqanaki, A. Szameit, and P. Walther, Integrated-optics heralded controlled-NOT gate for polarization-encoded qubits, *npj Quantum Inf.* **4**, 13 (2018).
- [6] J. P. Li, X. Gu, J. Qin, D. Wu, X. You, H. Wang, C. Schneider, S. Höfling, Y. H. Huo, C. Y. Lu, N. L. Liu, L. Li, and J. W. Pan, Heralded nondestructive quantum entangling gate with single-photon sources, *Phys. Rev. Lett.* **126**, 140501 (2021).
- [7] W. Q. Liu, H. R. Wei, and L. C. Kwek, Universal quantum multi-qubit entangling gates with auxiliary spaces, *Adv. Quantum Technol.* **5**, 2100136 (2022).
- [8] W. Q. Liu and H. R. Wei, Linear optical universal quantum gates with higher success probabilities, *Adv. Quantum Technol.* **6**, 2300009 (2023).
- [9] M. Luo and X. Wang, Universal quantum computation with qudits, *Sci. China Phys. Mech. Astron.* **57**, 1712 (2014).
- [10] Y. Wang, Z. Hu, B. C. Sanders, and S. Kais, Qudits and high-dimensional quantum computing, *Front. Phys.* **8**, 589504 (2020).
- [11] T. C. Ralph, K. J. Resch, and A. Gilchrist, Efficient Toffoli gates using qudits, *Phys. Rev. A* **75**, 022313 (2007).
- [12] B. P. Lanyon, M. Barbieri, M. P. Almeida, T. Jennewein, T. C. Ralph, K. J. Resch, G. J. Pryde, J. L. O’Brien, A. Gilchrist, and A. G. White, Simplifying quantum logic using higher-dimensional Hilbert spaces, *Nat. Phys.* **5**, 134 (2009).
- [13] W. Q. Liu and H. R. Wei, Optimal synthesis of the Fredkin gate in a multilevel system, *New J. Phys.* **22**, 063026 (2020).
- [14] W. Q. Liu, H. R. Wei, and L. C. Kwek, Low-cost Fredkin gate with auxiliary space, *Phys. Rev. Appl.* **14**, 054057 (2020).
- [15] E. T. Campbell, Enhanced fault-tolerant quantum computing in d -level systems, *Phys. Rev. Lett.* **113**, 230501 (2014).
- [16] M. Howard and E. Campbell, Application of a resource theory for magic states to fault-tolerant quantum computing, *Phys. Rev. Lett.* **118**, 090501 (2017).
- [17] H. Bechmann-Pasquinucci and W. Tittel, Quantum cryptography using larger alphabets, *Phys. Rev. A* **61**, 062308 (2000).
- [18] J. Cortese, Holevo-Schumacher-Westmoreland channel capacity for a class of qudit unital channels, *Phys. Rev. A* **69**, 022302 (2004).
- [19] P. B. Dixon, G. A. Howland, J. Schneeloch, and J. C. Howell, Quantum mutual information capacity for high-dimensional entangled states, *Phys. Rev. Lett.* **108**, 143603 (2012).
- [20] X. M. Hu, Y. Guo, B. H. Liu, Y. F. Huang, C. F. Li, and G. C. Guo, Beating the channel capacity limit for superdense coding with entangled ququarts, *Sci. Adv.* **4**, eaat9304 (2018).
- [21] N. J. Cerf, M. Bourennane, A. Karlsson, and N. Gisin, Security of quantum key distribution using d -level systems, *Phys. Rev. Lett.* **88**, 127902 (2002).
- [22] L. Zhang, C. Silberhorn, and I. A. Walmsley, Secure quantum key distribution using continuous variables of single photons, *Phys. Rev. Lett.* **100**, 110504 (2008).

- [23] F. Wang, P. Zeng, J. Zhao, B. Braverman, Y. Zhou, M. Mirhosseini, X. Wang, H. Gao, F. Li, R. W. Boyd, and P. Zhang, High-dimensional quantum key distribution based on mutually partially unbiased bases, *Phys. Rev. A* **101**, 032340 (2020).
- [24] D. Collins, N. Gisin, N. Linden, S. Massar, and S. Popescu, Bell inequalities for arbitrarily high-dimensional systems, *Phys. Rev. Lett.* **88**, 040404 (2002).
- [25] T. Vértesi, S. Pironio, and N. Brunner, Closing the detection loophole in Bell experiments using qudits, *Phys. Rev. Lett.* **104**, 060401 (2010).
- [26] A. C. Dada, J. Leach, G. S. Buller, M. J. Padgett, and E. Andersson, Experimental high-dimensional two-photon entanglement and violations of generalized Bell inequalities, *Nat. Phys.* **7**, 677 (2011).
- [27] L. Sheridan and V. Scarani, Security proof for quantum key distribution using qudit systems, *Phys. Rev. A* **82**, 030301 (2010).
- [28] Z. Liu and H. Fan, Decay of multiqudit entanglement, *Phys. Rev. A* **79**, 064305 (2009).
- [29] S. Ecker, F. Bouchard, L. Bulla, F. Brandt, O. Kohout, F. Steinlechner, R. Fickler, M. Malik, Y. Guryanova, R. Ursin, and M. Huber, Overcoming noise in entanglement distribution, *Phys. Rev. X* **9**, 041042 (2019).
- [30] M. Erhard, R. Fickler, M. Krenn, and A. Zeilinger, Twisted photons: new quantum perspectives in high dimensions, *Light: Sci. Appl.* **7**, 17146 (2018).
- [31] D. Cozzolino, B. Da Lio, D. Bacco, and L. K. Oxenløwe, High-dimensional quantum communication: benefits, progress, and future challenges, *Adv. Quantum Technol.* **2**, 1900038 (2019).
- [32] M. Erhard, M. Krenn, and A. Zeilinger, Advances in high-dimensional quantum entanglement, *Nat. Rev. Phys.* **2**, 365 (2020).
- [33] Y. Chi, Y. Yu, Q. Gong, and J. Wang, High-dimensional quantum information processing on programmable integrated photonic chips, *Sci. China Inf. Sci.* **66**, 180501 (2023).
- [34] M. S. Blok, V. V. Ramasesh, T. Schuster, K. O'Brien, J.-M. Kreikebaum, D. Dahlen, A. Morvan, B. Yoshida, N. Y. Yao, and I. Siddiqi, Quantum information scrambling on a superconducting qutrit processor, *Phys. Rev. X* **11**, 021010 (2021).
- [35] A. Cervera-Lierta, M. Krenn, A. Aspuru-Guzik, and A. Galda, Experimental high-dimensional Greenberger–Horne–Zeilinger entanglement with superconducting transmon qutrits, *Phys. Rev. Appl.* **17**, 024062 (2022).
- [36] M. Ringbauer, M. Meth, L. Postler, R. Stricker, R. Blatt, P. Schindler, and T. Monz, A universal qudit quantum processor with trapped ions, *Nat. Phys.* **18**, 1053 (2022).
- [37] B. Anderson, H. Sosa-Martinez, C. Riofrío, I. H. Deutsch, and P. S. Jessen, Accurate and robust unitary transformations of a high-dimensional quantum system, *Phys. Rev. Lett.* **114**, 240401 (2015).
- [38] Y. Fu, W. Liu, X. Ye, Y. Wang, C. Zhang, C. K. Duan, X. Rong, and J. Du, Experimental investigation of quantum correlations in a two-qutrit spin system, *Phys. Rev. Lett.* **129**, 100501 (2022).
- [39] A. Babazadeh, M. Erhard, F. Wang, M. Malik, R. Nouroozi, M. Krenn, and A. Zeilinger, High-dimensional single-photon quantum gates: concepts and experiments, *Phys. Rev. Lett.* **119**, 180510 (2017).
- [40] X. Gao, M. Krenn, J. Kysela, and A. Zeilinger, Arbitrary d -dimensional Pauli X gates of a flying qudit, *Phys. Rev. A* **99**, 023825 (2019).
- [41] X. Gao, M. Erhard, A. Zeilinger, and M. Krenn, Computer-inspired concept for high-dimensional multipartite quantum gates, *Phys. Rev. Lett.* **125**, 050501 (2020).
- [42] Y. Wang, S. Ru, F. Wang, P. Zhang, and F. Li, Experimental demonstration of efficient high-dimensional quantum gates with orbital angular momentum, *Quantum Sci. and Technol.* **7**, 015016 (2021).
- [43] P. Imany, J. A. Jaramillo-Villegas, M. S. Alshaykh, J. M. Lukens, O. D. Odele, A. J. Moore, D. E. Leaird, M. Qi, and A. M. Weiner, High-dimensional optical quantum logic in large operational spaces, *npj Quantum Inf.* **5**, 59 (2019).
- [44] F. Brandt, M. Hiekkamäki, F. Bouchard, M. Huber, and R. Fickler, High-dimensional quantum gates using full-field spatial modes of photons, *Optica* **7**, 98 (2020).
- [45] Y. Chi, J. Huang, Z. Zhang, J. Mao, Z. Zhou, X. Chen, C. Zhai, J. Bao, T. Dai, H. Yuan, M. Zhang, D. Dai, B. Tang, Y. Yang, Z. Li, Y. Ding, L. K. Oxenløwe, M. G. Thompson, J. L. O'Brien, Y. Li, Q. Gong, and J. Wang, A programmable qudit-based quantum processor, *Nat. Commun.* **13**, 1166 (2022).
- [46] Q. Zeng, T. Li, X. Song, and X. Zhang, Realization of optimized quantum controlled-logic gate based on the orbital angular momentum of light, *Opt. Express* **24**, 8186 (2016).
- [47] J. Lopes, W. Soares, B. de Lima Bernardo, D. Caetano, and A. Canabarro, Linear optical CNOT gate with orbital angular momentum and polarization, *Quantum Inf. Process.* **18**, 256 (2019).
- [48] H. Ke, S. Fang, and W. Zhang, A versatile device for implementing the optical quantum gates in multiple degrees of freedom, *Opt. Laser Technol.* **169**, 110137 (2023).
- [49] Y. Li, P. C. Humphreys, G. J. Mendoza, and S. C. Benjamin, Resource costs for fault-tolerant linear optical quantum computing, *Phys. Rev. X* **5**, 041007 (2015).
- [50] I. Tzitrin, T. Matsuura, R. N. Alexander, G. Dauphinais, J. E. Bourassa, K. K. Sabapathy, N. C. Menicucci, and I. Dhand, Fault-tolerant quantum computation with static linear optics, *PRX Quantum* **2**, 040353 (2021).
- [51] S. D. Bartlett, H. de Guise, and B. C. Sanders, Quantum encodings in spin systems and harmonic oscillators, *Phys. Rev. A* **65**, 052316 (2002).
- [52] B. Do, M. L. Stohler, S. Balasubramanian, D. S. Elliott, C. Eash, E. Fischbach, M. A. Fischbach, A. Mills, and B. Zwickl, Experimental realization of a quantum quincunx by use of linear optical elements, *J. Opt. Soc. Am. B* **22**, 499 (2005).
- [53] A. M. Childs, Universal Computation by Quantum Walk, *Phys. Rev. Lett.* **102**, 180501 (2009).
- [54] N. B. Lovett, S. Cooper, M. Everitt, M. Trevers, and V. Kendon, Universal quantum computation using the discrete-time quantum walk, *Phys. Rev. A* **81**, 042330 (2010).
- [55] F. Wang, M. Erhard, A. Babazadeh, M. Malik, M. Krenn, and A. Zeilinger, Generation of the complete four-dimensional Bell basis, *Optica* **4**, 1462 (2017).
- [56] M. Mafu, A. Dudley, S. Goyal, D. Giovannini, M. McLaren, M. J. Padgett, T. Konrad, F. Petruccione, N. Lütkenhaus, and A. Forbes, Higher-dimensional orbital-angular-momentum-based quantum key distribution with mutually unbiased bases, *Phys. Rev. A* **88**, 032305 (2013).

- [57] Y. H. Luo, H. S. Zhong, M. Erhard, X. L. Wang, L. C. Peng, M. Krenn, X. Jiang, L. Li, N.-L. Liu, C. Y. Lu, *et al.*, Quantum teleportation in high dimensions, *Phys. Rev. Lett.* **123**, 070505 (2019).
- [58] T. Feng, Q. Xu, L. Zhou, M. Luo, W. Zhang, and X. Zhou, Quantum information transfer between a two-level and a four-level quantum systems, *Photon. Res.* **10**, 2854 (2022).

Supplementary Materials for “Experimental realization of universal high-dimensional quantum gates with ultra-high fidelity and efficiency”

Zhe Meng,^{*} Wen-Qiang Liu,^{*} Bo-Wen Song, Xiao-Yun Wang, An-Ning Zhang,[†] and Zhang-Qi Yin[‡]

Center for Quantum Technology Research and Key Laboratory of
Advanced Optoelectronic Quantum Architecture and Measurements (MOE),
School of Physics, Beijing Institute of Technology, Beijing 100081, China

(Dated: December 1, 2023)

THE PROPOSALS FOR THE REALIZING THE FOUR DIMENSIONAL X_4 GATE, Z_4 GATE, AND ALL OF THEIR INTEGER POWERS.

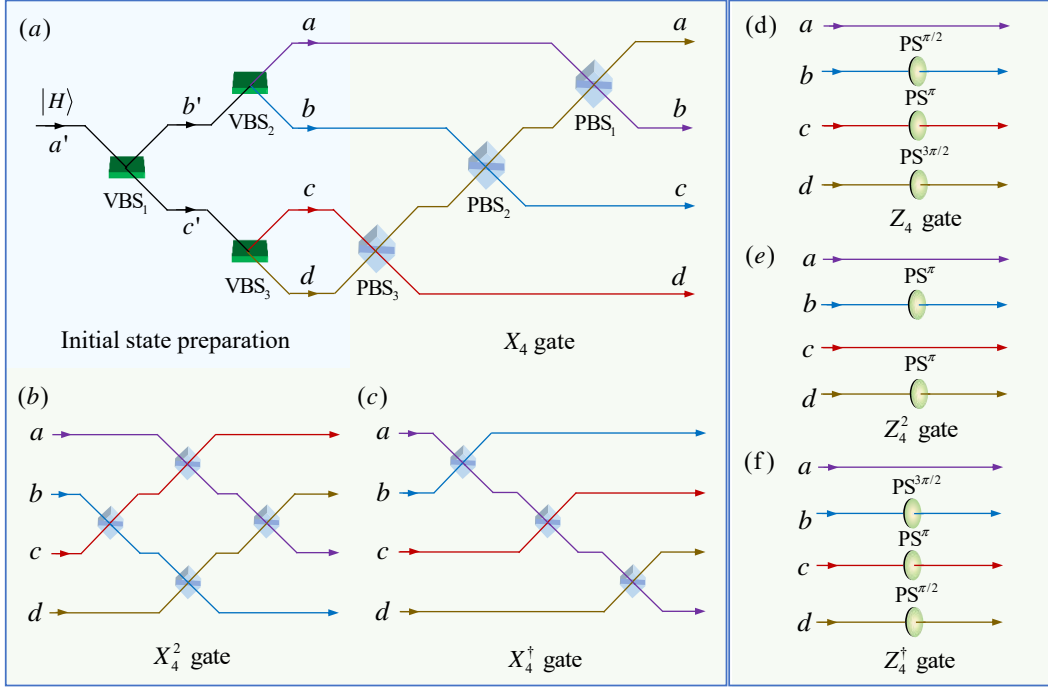


FIG. S1: Schematic proposals for realizing the four dimensional Pauli X_4 gate, Z_4 gate, and all of their integer powers. (a) The initial state preparation and the realization of the X_4 gate. A horizontally polarized photon $|H\rangle$ is injected in the spatial mode a' to prepare a general initial state by using three spatial variable beam splitters (VBSs). Then the photon is routed to a X_4 gate composed of three polarized beam splitters (PBSs). The PBSs change the spatial mode of the incident photon from $(|Ha\rangle, |Hb\rangle, |Hc\rangle, |Hd\rangle)$ to $(|Hb\rangle, |Hc\rangle, |Hd\rangle, |Ha\rangle)$, because each PBS transmits the H -polarized photon and reflects the vertically V -polarized photon. (b) The realization of the X_4^2 gate where the spatial mode of the photon is changed from $(|Ha\rangle, |Hb\rangle, |Hc\rangle, |Hd\rangle)$ to $(|Hc\rangle, |Hd\rangle, |Ha\rangle, |Hb\rangle)$. (c) The realization of the X_4^\dagger gate where the spatial mode of the photon is changed from $(|Ha\rangle, |Hb\rangle, |Hc\rangle, |Hd\rangle)$ to $(|Hd\rangle, |Ha\rangle, |Hb\rangle, |Hc\rangle)$. (d) The realization of the Z_4 gate. (e) The realization of the Z_4^2 gate. (f) The realization of the Z_4^\dagger gate. PS^θ denotes a phase shifter with the angle θ , which introduces a mode-dependent phase $e^{i\theta}$ in the corresponding spatial modes.

Figure. S1 shows the theoretical proposals for realizing four-dimensional Pauli X_4 gate, Z_4 gate, and all of their integer powers by encoding the gate qudit on the polarization-spatial degree of freedom of the single photons, i.e., $|0\rangle \leftrightarrow |Ha\rangle$, $|1\rangle \leftrightarrow |Hb\rangle$, $|2\rangle \leftrightarrow |Hc\rangle$, and $|3\rangle \leftrightarrow |Hd\rangle$. Here H is horizontally polarized state of photons and a, b, c, d are the spatial modes of the photon. As shown in Fig. S1(a), a horizontally polarized photon $|H\rangle$ is injected into the spatial mode a' to prepare the initial state. The $|Ha'\rangle$ photon firstly goes through a variable beam splitter (VBS₁) to be divided into two arms b' and c' , which evolves the photon state as

$$|Ha'\rangle \rightarrow r_1|Hb'\rangle + t_1|Hc'\rangle. \quad (S1)$$

Here the coefficients r_1 and t_1 are determined by the reflectivity and the transmittance of the VBS₁, respectively, and they satisfy $|r_1|^2 + |t_1|^2 = 1$. The photons in spatial modes b' and modes c' are transmitted and reflected at VBS₂ and VBS₃ to span a four-dimensional Hilbert space in spatial modes a, b, c , and d . The VBS₂ and VBS₃ change the state in Eq. (S1) as

$$r_1|Hb'\rangle + t_1|Hc'\rangle \rightarrow r_1t_2|Ha\rangle + r_1r_2|Hb\rangle + t_1r_3|Hc\rangle + t_1t_3|Hd\rangle. \quad (\text{S2})$$

Here the coefficients r_2, r_3, t_2 , and t_3 are determined by the reflectivity and the transmittance of the VBS₂ and VBS₃, respectively, and they satisfy $|r_2|^2 + |t_2|^2 = |r_3|^2 + |t_3|^2 = 1$. Because the reflectivity and the transmittance of the VBS₁, VBS₂, and VBS₃ can be adjusted arbitrarily [1], we denote $\alpha = r_1t_2$, $\beta = r_1r_2$, $\gamma = t_1r_3$, and $\delta = t_1t_3$, then Eq. (S2) is rewritten as

$$|\varphi_1\rangle = \alpha|Ha\rangle + \beta|Hb\rangle + \gamma|Hc\rangle + \delta|Hd\rangle. \quad (\text{S3})$$

Therefore, the initial state preparation is completed. In the Figs. 1(b)-(d) of the experimental setups in the main text, we realize the same functionality as VBS by using a combination of HWP, PBS, and HWP. The HWPs positioned before the PBS serve to modulate the polarization according to coefficients r_1 and t_1 . This modulation is mathematically represented as $|H\rangle \rightarrow \cos 2\theta|H\rangle + \sin 2\theta|V\rangle$, $|V\rangle \rightarrow \sin 2\theta|H\rangle - \cos 2\theta|V\rangle$, where θ signifies the angle of the optical axis of the HWP. Given that the PBS reflects the V -polarized photon and transmits the H -polarized photon, it can differentiate between the spatial modes of photons based on the ratio of H and V components. The HWP positioned after the PBS then transforms the polarization states of different spatial modes into the same H polarization, thereby fulfilling the role of a VBS.

The complex coefficients α, β, γ , and δ are determined by the reflectivity and the transmittance of the VBSs and satisfy the normalization condition $|\alpha|^2 + |\beta|^2 + |\gamma|^2 + |\delta|^2 = 1$. After the initial state is prepared, the photon is routed to a X_4 gate that is composed of three polarized beam splitters (PBS₁, PBS₂, and PBS₃). Because the PBS transmits H -polarized photon and reflects vertically V -polarized photon, the PBS₁, PBS₂, and PBS₃ evolve the initial state as

$$|\varphi_1\rangle \rightarrow \alpha|Hb\rangle + \beta|Hc\rangle + \gamma|Hd\rangle + \delta|Ha\rangle = |\varphi_{X_4}\rangle. \quad (\text{S4})$$

From Eq. (S3) to Eq. (S4), one can see that Fig. S1(a) realizes a X_4 gate. In this way, the X_4^2 gate and X_4^\dagger gate also can be realized by routing the photon to corresponding spatial modes using the PBSs, and the corresponding proposals are presented in Fig. S1(b) and Fig. S1(c), respectively.

The proposals for realizing the Z_4, Z_4^2, Z_4^\dagger gates are shown in Figs. S1(d)-(f), respectively. In order to realize these mode-dependent phase gates, we set some phase shifters (PS $^\theta$) rotated to an angle θ in the spatial modes to introduce a relative phase $e^{i\theta}$. As shown in Fig. S1(d), three phase shifters with the angles $\frac{\pi}{2}, \pi$, and $\frac{3\pi}{2}$ are placed respectively in the modes b, c , and d to realize the Z_4 gate. After the photon goes through three PSs, the initial state in Eq. (S3) is changed as

$$|\varphi_1\rangle \rightarrow \alpha|Hb\rangle + i\beta|Hc\rangle - \gamma|Hd\rangle - i\delta|Ha\rangle = |\varphi_{Z_4}\rangle. \quad (\text{S5})$$

In this way, the X_4^2 gate and X_4^\dagger gate also can be realized and they are presented in Fig. S1(e) and Fig. S1(f), respectively. In the Figs. 1(f)-(g) of the experimental setups in the main text, we use the sandwich structure of the wave plates group QWP1-HWP1-QWP2 to realize the PSs. The angles of the wave plates group required to achieve PS are presented in Tab. I.

TABLE I: The angles of the wave plates group to achieve the relative phase in our experimental setups.

phase $e^{i\theta}$	QWP 1	HWP1	QWP2
$\theta = 0$	0°	0°	0°
$\theta = \pi/2$	90°	0°	0°
$\theta = \pi$	0°	90°	0°
$\theta = 3\pi/2$	90°	90°	0°

THE RECONSTRUCTED DENSITY MATRICES FOR THE Z_4^2 GATE AND Z_4^\dagger GATE.

In order to assess the relative phase imparted by the Z_4^2 gate and Z_4^\dagger gate, we introduce an initial state $|\varphi\rangle = 1/2(|Ha\rangle + |Hb\rangle + |Hc\rangle + |Hd\rangle)$. We subsequently perform interferometry measurements on the spatial modes in

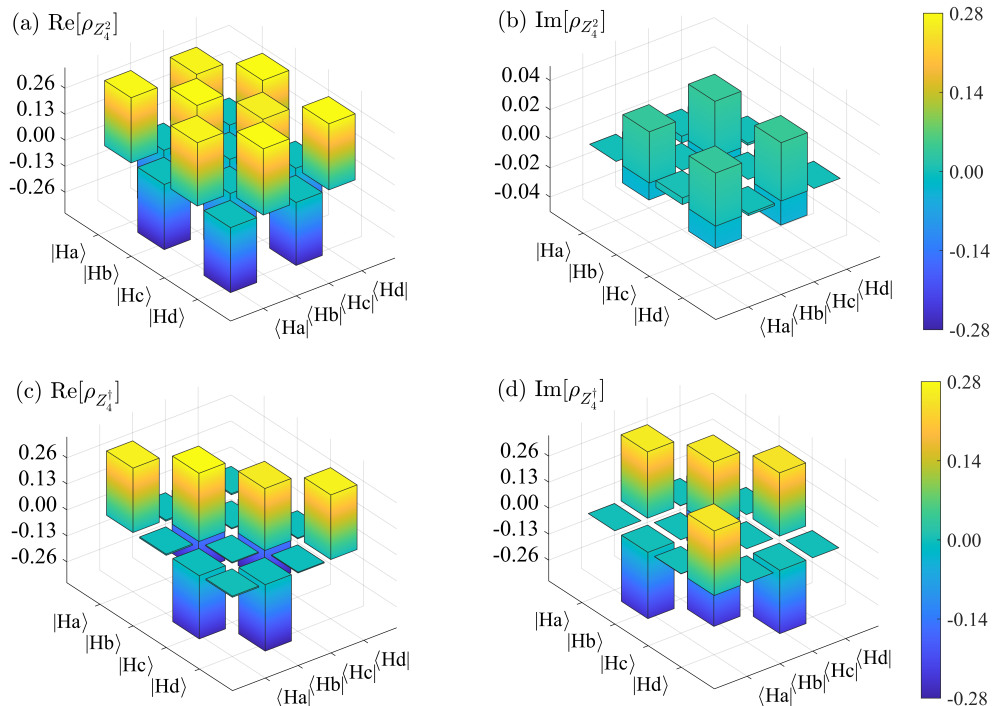


FIG. S2: The reconstructed density matrices $\rho_{Z_4^2}$ and $\rho_{Z_4^\dagger}$ for the Z_4^2 gate and Z_4^\dagger gate, respectively. (a) and (b) are the real part and the imaginary part of the density matrix for the Z_4^2 gate, respectively. (c) and (d) are the real part and the imaginary part of the density matrix for the Z_4^\dagger gate, respectively. The fidelities of the Z_4^2 gate and Z_4^\dagger gate are 99.55% and 99.83%, respectively.

pairs, such as a and b , c and d , b and c . The relative phase between two spatial modes is measured by the probability $P = 1/2(1 + \cos \theta)$ obtained from these measurements. In this way we measure the experimental coefficients α , β , γ , δ by the interference of photons in spatial modes a and b , c and d , b and c for a input equal superposition state and plot the reconstructed density matrices for the Z_4^2 gate and Z_4^\dagger gate in Fig. S2. The fidelities of the Z_4^2 gate and Z_4^\dagger gate are 99.55% and 99.83%, respectively.

THE PERFORMANCE OF THE CX_4 GATE, CX_4^2 GATE, AND CX_4^\dagger GATE.

We check the conversion efficiencies of the CX_4 gate, CX_4^2 gate, and CX_4^\dagger gate by preparing a qudit in one of the eight input computational basis $|Va\rangle, \dots, |Vd\rangle, |Ha\rangle, \dots, |Hd\rangle$. The probabilities of all output basis states are measured in 10s. The results of the conversion efficiencies are presented in Tab. II and the truth tables of them are plotted in Fig. S3. The average efficiencies of the CX_4^2 gate and CX_4^\dagger gate are 99.78% and 99.73%, respectively.

TABLE II: The in-out efficiency $\mathcal{P}(i, j)$ for the CX_4 , CX_4^2 , and CX_4^\dagger gates in our experimental setups.

Input mode	$ Va\rangle$	$ Vb\rangle$	$ Vc\rangle$	$ Vd\rangle$	$ Ha\rangle$	$ Hb\rangle$	$ Hc\rangle$	$ Hd\rangle$
CX_4 gate	98.95%	99.10%	99.70%	99.10%	99.19%	99.12%	99.56%	99.30%
CX_4^2 gate	99.03%	99.92%	99.61%	99.49%	99.19%	99.84%	99.96%	99.45%
CX_4^\dagger gate	99.30%	99.88%	99.47%	99.42%	99.32%	99.79%	99.50%	99.09%

* These two authors contributed equally to this work.

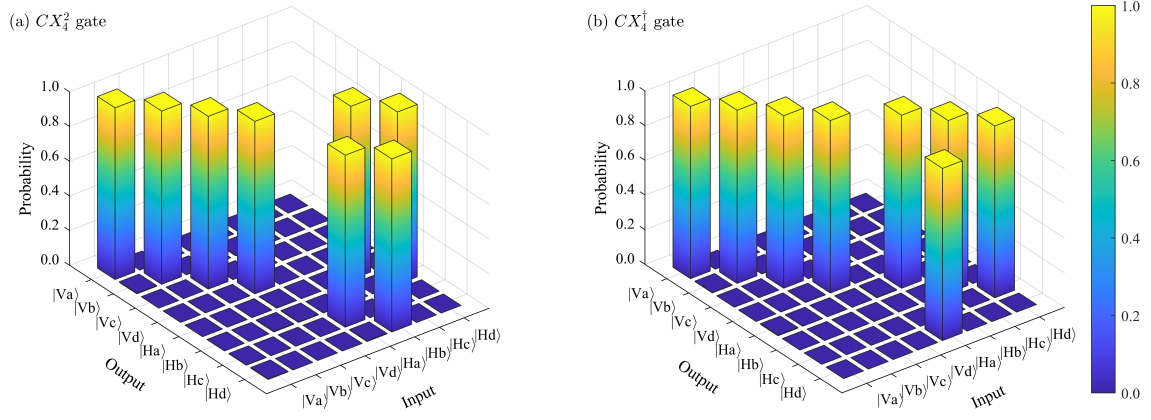


FIG. S3: Truth tables for the (a) CX_4^2 gate and (b) CX_4^\dagger gate. The average efficiencies of the CX_4^2 gate and CX_4^\dagger gate are 99.78% and 99.73%, respectively.

[†] Electronic address: Corresponding author. Anningzhang@bit.edu.cn

[‡] Electronic address: Corresponding author. zqyin@bit.edu.cn

- [1] M. Reck, A. Zeilinger, H. J. Bernstein, and P. Bertani, Experimental realization of any discrete unitary operator, Phys. Rev. Lett. **73**, 58 (1994).